Different thermal fatigue behaviors between gray cast iron and vermicular graphite cast iron

Gui-quan Wang[1], Zhong-li Liu[1], Yan-xiang Li[2, 3], and *Xiang Chen[2, 3]

1. School of Nuclear Equipment and Nuclear Engineering, Yantai University, Yantai 264005, Shandong, China

2. School of Materials Science and Engineering, Tsinghua University, Beijing 100084, China

3. Key Laboratory for Advanced Materials Processing Technology, Ministry of Education, Tsinghua University, Beijing 100084, China

Abstract: The initiation and propagation of thermal fatigue cracks in gray cast iron and vemicular graphite cast iron were investigated by Uddeholm method to reveal the complex thermal fatigue behaviors of cast iron. Differences of thermal fatigue behaviors of gray cast iron and vemicular graphite cast iron were observed and analyzed. It is found that the observed differences are related to the combination of graphite morphology and the oxidization of matrix. More oxidized matrix is observed in gray cast iron due to its large specific surface area. The brittle oxidized matrix facilitates the propagation of microcracks along the oxidization layer. By contrast, the radial microcracks are formed in vermicular graphite at the edge of graphite due to fewer oxidization layers. It indicates that the thermal fatigue resistance of gray cast iron is dominated by graphite content and morphology while that of vermicular graphite cast iron strongly relates to the strength of the matrix.

Keywords: thermal fatigue; gray cast iron; vermicular graphite cast iron; oxidization; cracking propagation

CLC numbers: TG143 **Document code:** A **Article ID:** 1672-6421(2022)03-245-08

1 Introduction

With alternating firing load and frequent start-stop events, the vital structural components of automobiles (such as cylinder head, brake disc and exhaust manifold) are mainly subjected to periodic thermal stress. The fracture of these components is usually referred to thermal fatigue or thermal shock when the heating/cooling rate is rapid [1-3].

Typical casting materials with high thermal fracture endurance are gray cast iron (GCI) and vermicular graphite cast iron (VGI). GCI has been widely used for many years owing to its excellent thermal conductivity, castability and the best compromise between feasibility and cost [4-6]. VGI is expected to substitute GCI because of improved strength, good ductility, less crack nucleation sites resulted by the rounded vermicular graphite [7, 8].

However, the preceding literature revealed contradictory results about the thermal fatigue resistance of GCI and VGI. The thermal fracture endurance of pig iron ingots manufactured with different cast irons has been tested [9]. Results showed that VGI provides better thermal fatigue resistance than GCI due to the higher strength-to-thermal stress ratio. A similar conclusion was reported by Ruff [10] and Lee [11] based on experimental analysis. By contrast, Fredriksson [12] concluded that GCI has better resistance to thermal fatigue due to its lower elasticity modulus and higher heat diffusivity. Zieher [13] and Nechtelberger [14] obtained results similar to Fredriksson's.

The contradictory conclusion of the above studies can be explained by the complex thermal fatigue behavior and inhomogeneous structure of cast iron. Many studies have pointed out that thermal fatigue fracture is affected by many properties, such as thermal conductivity, tensile strength, and Young's modulus [15-17]. Furthermore, the nucleation and propagation of thermal cracks are strongly related to the structural characteristics. Zhang et al. [18] suggested that the pearlite content of VGI has important influences on its thermal fatigue resistance. Wang and Zhang [19] found that the graphite content and morphology affect the oxidation and thermal cracking behavior of VGI. Lan and Zhang [20, 21] studied the thermal fatigue of gray iron mold by experiment and simulation. Their results suggested that the matrix strength and graphite morphology dominate the mold's service life. The chemical compositions can also affect the thermal fatigue resistance of cast irons by changing their strength and structure [22-24]. However,

***Xiang Chen**

Male, born in 1970, Professor. His research and teaching interests are focused on the areas of cast alloying materials and porous metal materials.

E-mail: xchen@tsinghua.edu.cn

Received: 2021-11-11; Accepted: 2022-04-11

there are limited studies to simultaneously investigate the thermal cracking behaviors of GCI and VGI and reveal the key factors for improving their thermal fatigue resistance.

In this work, thermal fatigue endurance of GCI and VGI with different structures and properties was tested based on the self-restraint Uddeholm method. The influences of structures and properties were analyzed by the initiation and propagation of thermal fatigue cracks, and the different thermal cracking behaviors of GCI and VGI were discussed based on the observation.

2 Experimental details

2.1 Materials

GCIs and VGIs were prepared using a 500 kg medium frequency induction furnace. The charge materials included steel scrap, pig iron, ferro-molybdenum, ferro-silicon and carburizer. The melts were superheated to 1,530 °C for about 5 min and then transferred into a ladle. GCIs were inoculated by FeSiSr (0.40wt.%) which is deposited at the bottom of ladle before pouring. VGIs were treated by the sandwich vermicularizing method with vermicularizing agent FeSiMgCe (0.35wt.%) and inoculant FeSiBa (0.40wt.%). The GCI samples were cast in EN-1561 Type II molds, while the VGI samples were made in ISO 16112:2006 Type IIb mold. The chemical compositions of samples are listed in Table 1. For GCIs, C content was changed to obtain different thermal conductivities by changing the contents and sizes of graphite flakes, while Mo (about 0.35wt.%) and Sn (about 0.06wt.%) were used to keep high tensile strength by promoting and strengthening pearlitic matrix. For VGI, high Si content (about 2.4wt.%) was used to improve the casting properties, while contents of C, Mo and Sn were changed to obtain various combinations of tensile strength and thermal conductivity.

Table 1: Chemical compositions of samples

	No.	C	Si	Mn	P	S	Cu	Mo	Sn	Mg	Ce
GCI	G1	3.39	1.64	0.46	0.025	0.030	0.55	0.35	0.057	-	-
	G2	3.58	1.62	0.50	0.029	0.028	0.54	0.33	0.059	-	-
	G3	3.69	1.59	0.51	0.030	0.027	0.58	0.35	0.061	-	-
VGI	V1	3.53	2.42	0.58	0.012	0.030	0.42	0.19	0.002	0.018	0.011
	V2	3.51	2.37	0.56	0.021	0.030	0.42	-	0.014	0.016	0.008
	V3	3.60	2.40	0.38	0.010	0.033	0.41	0.22	-	0.015	0.009

2.2 Mechanical and physical properties

According to the Chinese Standard GB/T 228.1-2010, tensile tests were performed for each composition at room temperature. The test bars were 140 mm in length with a 20 mm gauge diameter. Young's modulus and Poisson's ratio were measured using a resonant ultrasound spectrometer (Magnaflux Quasar System) with cylindrical specimens (8 mm in diameter and 10 mm in length). The thermal expansion coefficient was measured by a Hengjiu HPY-1 thermal dilatometer at a heating rate of 10 ºC·min^{-1} from 25 ºC to 600 ºC. Disk specimens with 12.5 mm in diameter and 2.5 mm in thickness were used to determine the thermal diffusivity (a) and heat capacity (c_p) using a NETZSCH LFA 457 laser flash apparatus. The volume of the specimen was measured by the Archimedes method. The density (ρ) was calculated by weighting the specimen and dividing it by the volume. Then, the thermal conductivity (λ) was calculated by Eq. (1):

$$\lambda = a\rho c_p \tag{1}$$

2.3 Microstructural characterization

The disk specimens used for thermal conductivity measurement were then repolished and prepared for metallographic observation. The length and area percentage of graphite flakes were evaluated by quantitative metallography with Image J Pro software. The average of the three longest flakes in a field of view was measured according to Chinese Standard GB/T 7216-2009 since most of the graphite flakes are incomplete in a random 2D section. The average value of nine flakes in three typical fields was taken as the graphite length. The nodularity of VGI was estimated based on ISO 16112:2017, and the vermicularity was calculated by (1–nodularity)×100. The GCI and VGI specimens were then etched by 4% nital for 5 s to reveal the pearlite and ferrite. The ratio of pearlite to ferrite was calculated by the quantitative metallography with Image J Pro. A total of eight fields were calculated and the average value was taken.

2.4 Thermal fatigue test

The Uddeholm method was developed based on the high-frequency heating of a small cylindrical specimen [25]. The thermal fatigue tester is schematically shown in Fig. 1. K-type thermocouple wires with 0.13 mm in diameter were welded to the middle position of specimens to measure the surface temperature. The specimens were heated by magnetic induction and cooled by cooling water. The thermal cycling was designed as follows: temperature range: 45±5 ºC to 560±5 ºC; heating time: 3.6 s; holding time 1 s; cooling time: 1.4 s; holding time:

3.8 s; number of cycles: 1,000.

The specimens subjected to thermal fatigue were then washed with 15% hydrochloric acid solution. The surface cracks were observed by an Olympus SZ61 stereomicroscope and a JEOL field-emission scanning electron microscope (SEM) with an energy dispersive spectrometer (EDS). After the specimens were cut in the center, the cross-sections were observed by SEM to analyze the cracking propagation.

Then, the characteristics of thermal fatigue cracks were summarized as follows:

(1) The continuous network of surface macrocracks was defined as reticular cracks. A grid was superimposed on the micrographs obtained by the stereomicroscope. The intersections of the grid and reticular surface cracks were counted. The density of reticular cracks was defined as the average number of intersections per 1 mm length. Three micrographs were measured and the average density was taken to improve the precision.

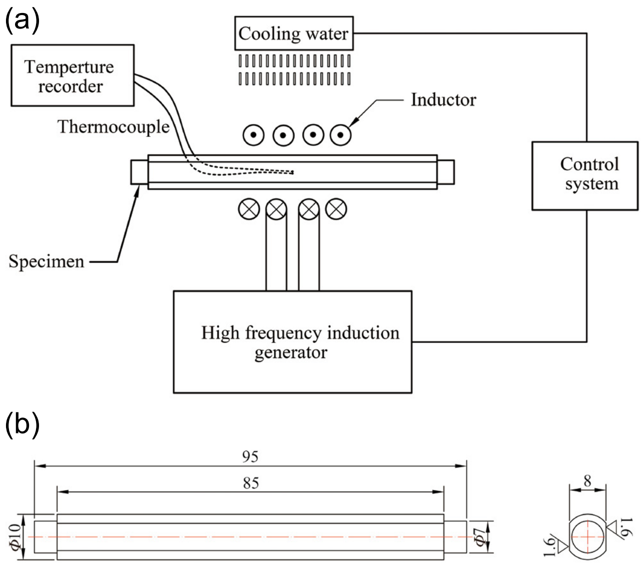

Fig. 1: Thermal fatigue test based on the Uddeholm method: (a) schematic diagram of thermal fatigue test; (b) dimension of specimen (unit: mm)

(2) The cracks on the cross-sections of the specimen were defined as longitudinal cracks. The average length of the three longest cracks on 3 SEM images was taken as the length of longitudinal cracks.

3 Results and discussion

3.1 Mechanical and physical properties

Six cast irons (G1–G3 for GCI and V1–V3 for VGI) with different structures and properties were obtained by changing the inoculation process and chemical composition, as shown in Table 2. Typical microstructures of GCIs and VGIs are shown in Fig. 2. Homogeneous structures consisting of a fully pearlitic matrix and evenly distributed A-type graphite are observed in all GCIs. The differences of properties between GCI and VGI mainly exist in tensile strength and thermal conductivity. Generally, GCI performs higher thermal conductivity but lower tensile strength and Young's modulus. This is indeed expected since the lamellar graphite of GCI is longer and sharper [4-6, 19-21]. There is a contradictory relationship between tensile strength and thermal conductivity of cast irons, which is also expected since graphite provides high heat conduction, but reduces the strength. The ranges of tensile strength and thermal conductivity of cast irons are respectively (285.1–500.0 MPa) and (29.1–69.8 $W \cdot m^{-1} \cdot K^{-1}$), which are wide enough to reflect their effects on the thermal fatigue resistance.

3.2 Thermal fatigue cracks

The thermal fatigue cracks on the surface of GCI are presented in Fig. 3. Uniform reticular cracks are observed on the surface of G1 and G2. The cracking network of G1 seems denser than that of G2. No obvious cracks are observed on the surface of G3 in the view of stereomicroscope. The morphologies of thermal fatigue cracks of GCI on the polished cross-sections are also shown in Fig. 3. Bent and long longitudinal cracks are observed on G1 and G2 while short longitudinal cracks appear on G3. In consideration of no reticular cracks observed in Fig. 3(e), G3

Table 2: Structures and properties of the samples at room temperature (mean values)

Structures/properties	G1	G2	G3	V1	V2	V3
Graphite percentage (%)	8.6	9.4	9.9	8.8	8.7	9.6
Graphite length (μm)	214.2	221.3	260.1	-	-	-
Pearlit/ferrite ratio	-	-	-	0.47	3.93	0.51
Vermicularity (%)	-	-	-	78.9	85.5	80.5
Tensile strength (MPa)	315.5	293.7	285.1	370.5	411.5	500.0
Thermal conductivity ($W \cdot m^{-1} \cdot K^{-1}$)	47.8	51.4	61.8	34.6	37.1	29.1
Young's modulus (GPa)	138.8	138.6	131.3	158.6	149.8	166.6
Poisson ratio	0.28	0.27	0.27	0.27	0.28	0.28
Thermal expansion coefficient (10^{-6} K^{-1})	12.7	12.3	12.9	14.1	13.9	14.4

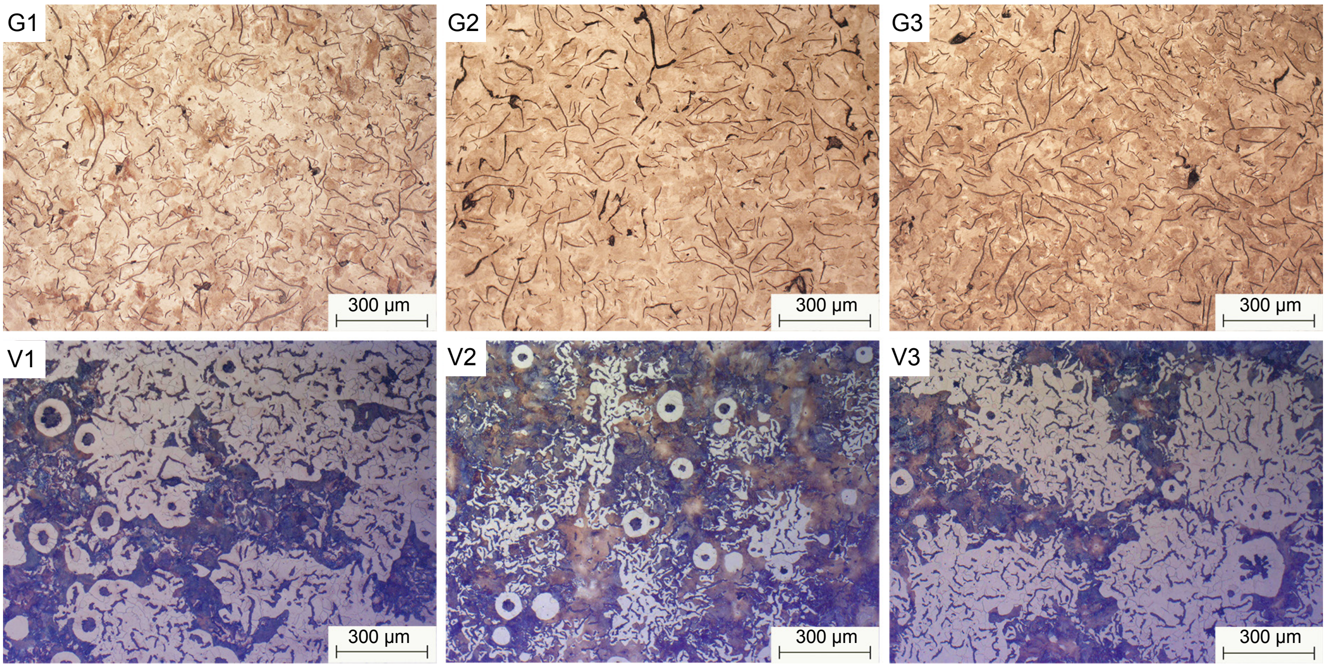

Fig. 2: Typical images showing microstructures of GCIs and VGIs

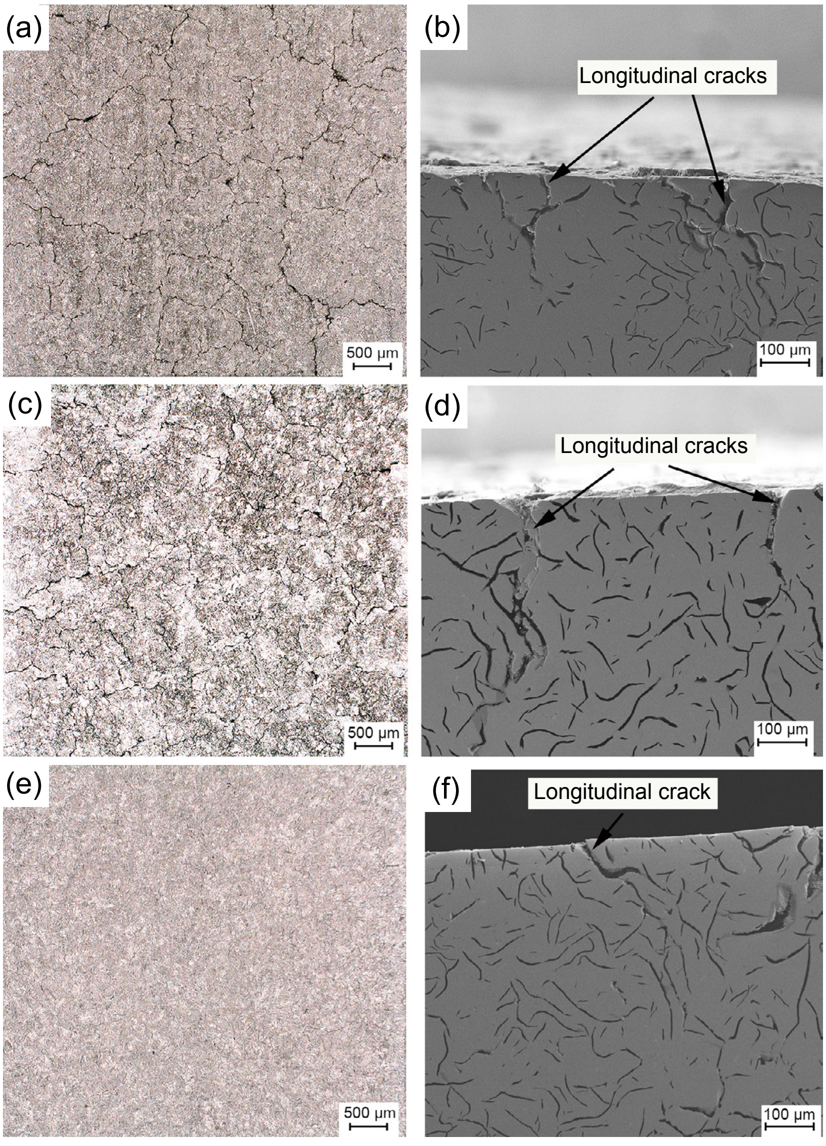

Fig. 3: Thermal fatigue cracks on the surface of G1 (a), G2 (c), G3 (e) and cross-section of G1 (b), G2 (d), G3 (f)

shows the slightest thermal fracture. This could be attributed to its high thermal conductivity which reduces the temperature difference and thermal stress. Moreover, the bent longitudinal cracks propagates along the graphite flakes or occupies the locations of graphite particles after the oxidation of graphite. It implies that the propagation of cracks is strongly related to the distribution of graphite flakes.

The thermal fatigue cracks of VGI specimens are shown in Fig. 4. Dense reticular cracks appear on the surface of V1–V3. The most serious surface thermal fatigue cracking is found on V1 since there are many microcracks observed in the main network of cracks. The longitudinal cracks of VGI seem straighter and coarser comparing to that of GCI. All the longitudinal cracks of VGIs are almost perpendicular to the outside surface.

To quantify the characteristics of cracks, the density of reticular cracks and the length of longitudinal cracks were summarized and the results are listed in Fig. 5. The densest reticular cracks appear on V1 followed by G2. G1, V2 and V3 produces similar surface reticular cracks. On the other hand, the longest longitudinal cracks are also found on G2 followed by V1. The longitudinal cracks of G1 are slightly longer than V2 and V3. G3 has the fewest reticular cracks and the shortest longitudinal cracks. These comparisons indicate that G2 and V1 provide the worst thermal fatigue resistance while G3 performs the optimal thermal fatigue endurance. G1 has a similar thermal fatigue performance to V2 and V3.

Thus, the results of the present work show that the thermal fatigue resistance of cast irons is not only dominated by graphite shape but also affected by properties. GCI with high thermal conductivity can exhibit higher thermal fatigue resistance than conventional VGI due to reduced thermal stress, such as G3. Conversely, VGI with high tensile strength can increase the resistance to thermal stress to compensate the negative effect of low thermal conductivity, such as V3.

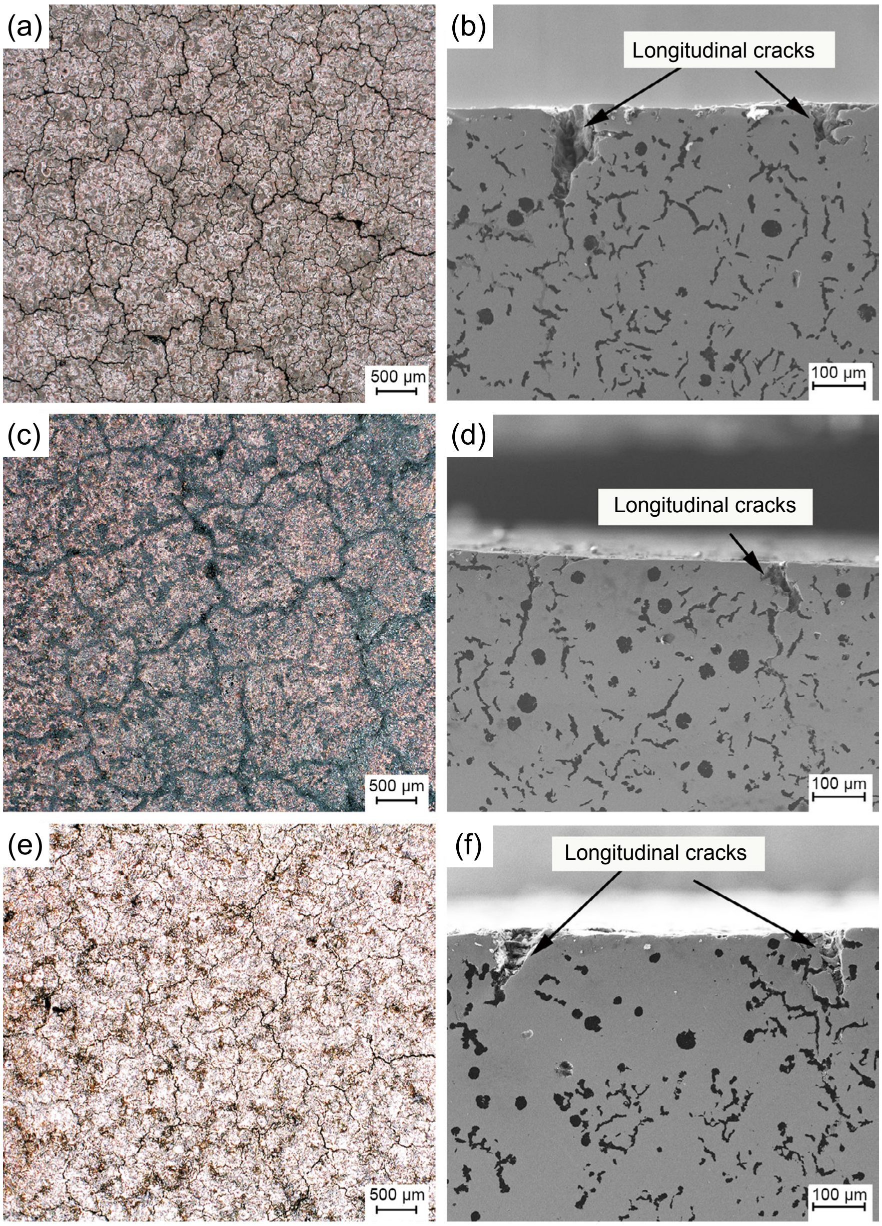

Fig. 4: Thermal fatigue cracks on the surface of V1 (a), V2 (c), V3 (e) and cross-section of V1 (b), V2 (d), V3 (f)

3.3 Initiation and propagation of cracks

In order to investigate the relationship between the properties and thermal cracking features, the thermal cracking behavior was analyzed based on SEM observations. Typical images of surface cracks are exhibited in Fig. 6. It is clear that cracks nucleate from the graphite edge in either GCI or VGI. This can be explained by the weak interface and different thermal expansions between graphite and ferritic matrix.

Figure 7 shows the details of longitudinal cracks of GCI. In Fig. 7(a), the main crack disappears at one end of graphite flake and emerges again at another side. It suggests that the main cracks propagate along with the graphite flakes. The graphite flakes near the main cracks are surrounded by an oxidization layer with a thickness of 2–4 μm according to the EDS results in Fig. 7 (Point A). The ferritic matrix can be oxidized during the thermal cycling by the reaction: $x\text{Fe} + y\text{O} \rightarrow \text{Fe}_x\text{O}_y$ [19, 26]. Oxidization bridges (paths) can also be observed between the graphite flakes, which implies that oxidized layers could be interconnected in the area of adjacent flakes with small spaces. Moreover, many fine microcracks are observed in the oxidized matrix near the main crack. As shown in Fig. 7(b), these microcracks can propagate among different graphite flakes through the oxidized matrix. It suggests the oxidized matrix provides a brittle channel for the propagation of microcracks and the formation of main cracks.

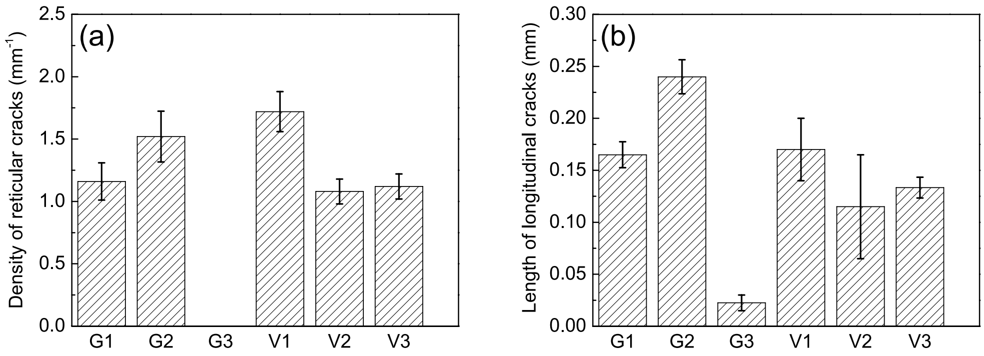

Fig. 5: Summarization of the density of reticular cracks (a) and the length of longitudinal cracks (b)

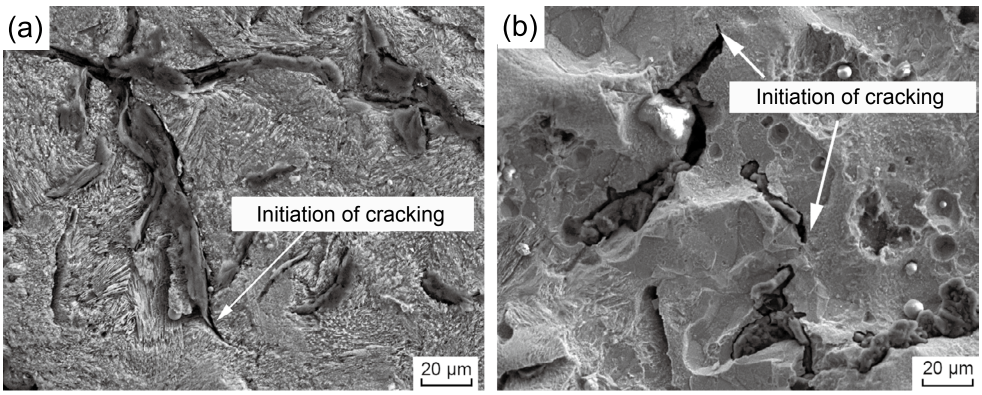

Fig. 6: Surface cracks of GCI (a) and VGI (b)

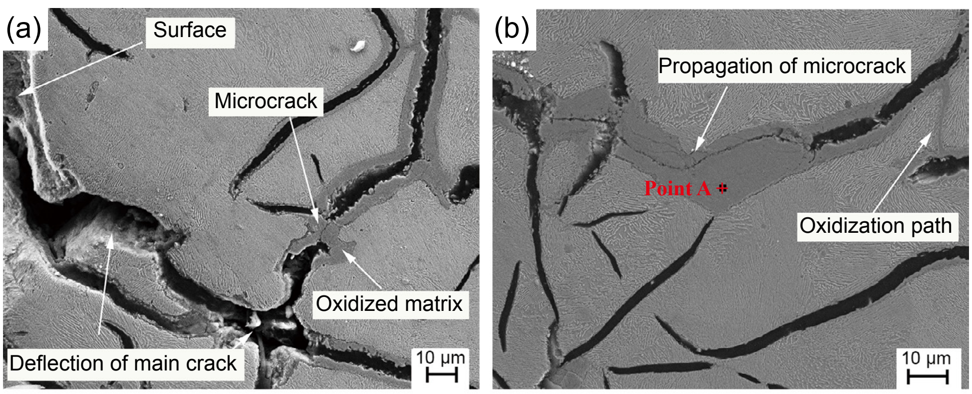

Point A	C	Si	O	Fe
wt.%	5.40	2.08	33.27	59.25
at.%	12.27	2.02	56.75	28.96

Fig. 7: Longitudinal cracks of GCI

The magnifications of longitudinal cracks of VGI are shown in Fig. 8. Similar to GCI, main cracks in VGI can deflect along the vermicular graphite and propagate in the oxidized matrix. The compositions of oxidized matrix in Fig. 8 are also comparable to that of GCI. However, fewer oxidization bridges (paths) are observed in VGI specimens, only a few graphite phases are surrounded by the oxidized matrix. These can be explained by the small specific area and large spacing of graphite particles. Moreover, most of the microcracks are radial from the graphite edge to the unoxidized matrix rather than propagate in the oxidized matrix. This implies that cracks propagate straightly from the graphite/matrix interface to the unoxidized matrix to relieve the thermal stress since few brittle oxidization bridges formed in VGI. The soft ferrite surrounding the vermicular graphite may make the cracks propagate easier.

The above observations indicate the different mechanisms of thermal fatigue cracking propagation in GCI and VGI. Figure 9 shows the diagrammatic sketch of the initiation and propagation of thermal fatigue cracks for GCI. When the thermal cycling loads increase, the cracks nucleate at the interface between graphite and matrix due to their different thermal expansions [Fig. 9(a)]. The nucleated cracks provide channels for oxygen diffusion from the ambient into the material, resulting in the oxidization layer around the lamellar graphite [Fig. 9(b)]. Then, the main crack is formed by propagating the cracks along the brittle oxidized matrix [Fig. 9(c)]. The graphite inside the main cracks may be broken or oxidized [26]. After that, more oxygen diffuses into the materials through the main cracks, leading to more diffusion paths and oxidized layers. Then, the main cracks continue to grow and deflect along the oxidized matrix between different graphite flakes, as shown in Fig. 9(d) and Fig. 9(e). This process indicates that the thermal fatigue behavior of GCI is dominated by the content and morphology of graphite flakes. Both the higher graphite content and longer graphite length lead to the increased thermal conductivity and thus the decreased thermal stress. However, they also provide more crack sources, more channels for oxidization and the smaller spacing between adjoining flakes, all of which would favor the thermal damage.

For VGI, the initiation of thermal fatigue cracks is similar to GCI as shown in Fig. 10(a) and Fig. 10(b). The cracks appear at the interface between graphite and matrix and make

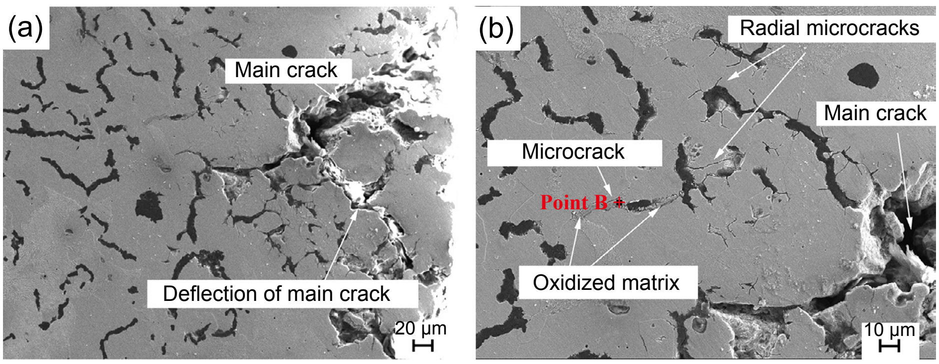

Point B	C	Si	O	Fe
wt.%	5.34	1.38	33.13	60.15
at.%	12.23	1.35	56.90	29.52

Fig. 8: Longitudinal cracks of VGI

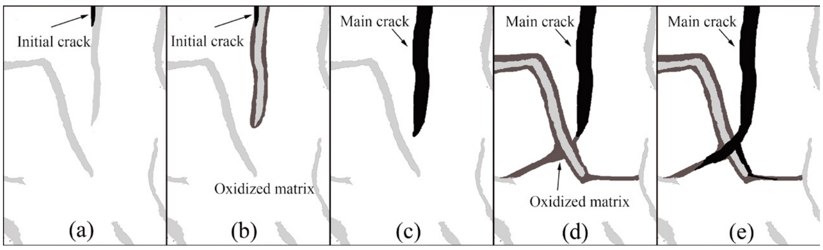

Fig. 9: Diagrammatic sketch of thermal cracking damage of GCI

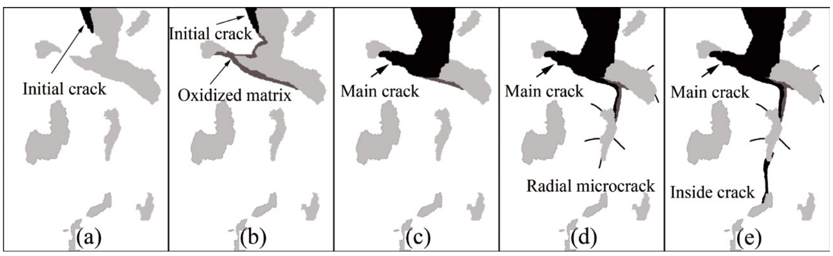

Fig. 10: Diagrammatic sketch of thermal cracking damage of VGI

the diffusion of oxygen easy to form oxidized matrix layer. However, fewer oxygen diffusion channels are formed because of the smaller specific area of vermicular graphite and thus the larger distance between adjoining graphite particles. The microcracks propagate straightly into the unoxidized matrix to relieve thermal stress when the thermal cycling loads increase [Fig. 10(d)]. Then, the cracks can further propagate along the radial microcracks [Fig. 10(e)]. It suggests the thermal fatigue behavior of VGI is different from that of GCI. The thermal fatigue resistance of VGI depends on two aspects: morphology of graphite and strength of the matrix. Moderate content and length of vermicular graphite can reduce the thermal stresses by high thermal conductivity and provide few brittle oxidation paths. The matrix with high strength can provide high resistance to prevent the formation of radial microcracks and the propagation of main cracks [27, 28].

4 Conclusions

Based on the Uddeholm method, the thermal fatigue of gray cast iron and vermicular graphite cast iron with various structures and properties was studied. The conclusions are summarized as follows:

(1) Thermal fatigue resistance of cast iron depends on its structure and properties rather than only the type of graphite. Gray cast iron with a combination of high thermal conductivity and tensile strength can provide higher thermal fatigue resistance compared with conventional vermicular graphite cast iron.

(2) The dominant factor of GCI's thermal damage is the graphite morphology. An appropriate combination of graphite content and length can provide improved thermal conductivity to reduce the thermal stress and suppress oxidization, so as to decelerate the propagation of cracks.

(3) The thermal fatigue behavior of VGI is different from that of GCI since the small specific area of vermicular graphite mitigates the matrix's oxidization. In absence of the oxidized matrix, the cracks will propagate straightly to the matrix to relieve thermal stress. The thermal fatigue resistance of VGI can be improved by strengthening the matrix.

References

[1] Riposan L, Chisamera M, Stan S. New developments in high quality grey cast Irons. China Foundry, 2014, 11(4): 351–364.
[2] Bertodo R. Grey cast irons for thermal-stress applications. Journal of Strain Analysis, 1970, 5(2): 98–109.
[3] Langmayr F, Zieher F, Lampic M. The thermo-mechanics of cast iron for cylinder heads. MTZ worldwide, 2004, 65(4): 17–20.
[4] Wang G H, Li Y X. Thermal conductivity of cast iron – A review. China Foundry, 2020, 17(2): 85–95.
[5] Helsing J, Grimvall G. Thermal conductivity of cast iron: Models and analysis of experiments. Journal of Applied Physics, 1991, 70(3): 1198–1206.
[6] Moonesan M, Raouf A H, Madah F, et al. Effect of alloying elements on thermal shock resistance of gray cast iron. Journal of Alloys and Compounds, 2012, 520: 226–231
[7] Dawson S, Schroeder T. Practical applications for compacted graphite iron. Transactions of the American Foundrymen's Society, 2004, 47(5): 1–9.
[8] Xu D M, Wang G Q, Chen X, et al. Effects of alloy elements on ductility and thermal conductivity of compacted graphite iron. China Foundry, 2018, 15(3): 189–195.
[9] Lee J, Lee S. Thermal fracture endurance of cast irons with application study of pig iron ingot molds. Metallurgical and Materials Transactions A, 1995, 26(6): 1431–1440.
[10] Ruff G F, Wallace J F. Control of graphite structure and its effect on mechanical properties of gray iron. Transactions of the American Foundry Society, 1976, 84: 705–728.
[11] Lee S, Weng L C. On thermal shock resistance of austenitic cast irons. Metallurgical and Materials Transactions A, 1991, 22(8): 1821–1831.
[12] Fredriksson H, Sunnerkrantz P, Ljubinković P. Relationship between structure and thermal fatigue in cast iron. Materials Science and Technology, 1988, 4(3): 222–226.
[13] Zieher F, Langmayr F, Jelatancev A, et al. Thermal mechanical fatigue simulation of cast iron cylinder heads. SAE Technical Paper, 2005, 25(7): 641–645.
[14] Nechtelberger E. Systematic Invenstigations to improve the quality of cylinder head cast iron with special reference to the tendency of crack formation. Oesterreichishes Giesseti Institute, 1975, 22: 733–738. (In German)
[15] Rukadikar M C, Reddy G P. Thermal fatigue resistance of alloyed pearlitic flake graphite irons. International Journal of Fatigue, 1987, 9(1): 25–34.
[16] Eichelberg G. Some new investigations on old combustion engine problems. Engineering, 1939, 148: 547–550.
[17] Hasselman D. Elastic energy at fracture and surface energy as design criteria for thermal shock. Journal of the American Ceramic Society, 1963, 46(11): 535–540.
[18] Zhang M X, Pang J C, Meng L J, et al. Study on thermal fatigue behaviors of two kinds of vermicular graphite cast irons. Materials Science & Engineering A, 2021, 814: 1–10.
[19] Wang X S, Zhang W Z. Oxidation and thermal cracking behavior of compacted graphite iron under high temperature and thermal shock. Oxidation of Metals, 2017, 87: 179–188.
[20] Lan P, Zhang J Q. Strength, microstructure and chemistry of ingot mould grey iron after different cycles of low frequency high temperature loads. Materials and Design, 2014, 54: 112–120.
[21] Lan P, Zhang J Q. Study on the mechanical behaviors of grey iron mould by simulation and experiment. Materials & Design, 2014, 53: 822–829.
[22] Pan S N, Zeng F Z, Su N G, et al. The effect of niobium addition on the microstructure and properties of cast iron used in cylinder head. Journal of Materials Research and Technology, 2020, 9(2): 1509–1518.
[23] Ding X F, Huang H, Matthias W, et al. Development of high performance cast iron with combination of improved mechanical and thermal properties through mo addition. Metallurgical and Materials Transactions A, 2018, 49(8): 3173–3177.
[24] Ding X F, Li X Z, Huang H, et al. Effect of mo addition on as-cast microstructures and properties of grey cast irons. Materials Science and Engineering A, 2018, 718: 483–491.
[25] Hu X B, Li L, Wu X C, et al. Coarsening behavior of $M_{23}C_6$ carbides after ageing on thermal fatigue in AISi H13 steel with niobium. International Journal of Fatigue, 2006, 28(3): 175–182.
[26] Ghodrat S, Janssen M, Kestens L, et al. Volume expansion of compacted graphite iron induced by pearlite decomposition and the effect of oxidation at elevated temperature. Oxidation of Metals, 2013, 80(1–2): 161–176.